Near-Infrared Window II Fluorescence Image-Guided Surgery of High-Grade Gliomas Prolongs the Progression-Free Survival of Patients

Xiaojing Shi, Zhe Zhang, Zeyu Zhang, Caiguang Cao, Zhen Cheng, Zhenhua Hu, *Senior Member, IEEE*, Jie Tian, *Fellow, IEEE*, and Nan Ji

Manuscript received June 14, 2021; revised September 22, 2021 and November 8, 2021; accepted November 16, 2021. Date of publication November 24, 2021; date of current version May 20, 2022. This study was supported in part by the National Key Research and Development Program of China under Grants 2017YFA0205200 and 2017YFC1309100, in part by the National Natural Science Foundation of China (NSFC) under Grants 62027901, 81930053, 92059207, 81227901, and 81930048, in part by the Beijing Natural Science Foundation under Grant JQ19027, in part by the Strategic Priority Research Program of the Chinese Academy of Sciences (XDA16021200), in part by the innovative research team of high-level local universities in Shanghai, in part by the Zhuhai High-level Health Personnel Team Project under Grant Zhuhai HLHPTP201703, and in part by the Capital characteristic clinical application project under Grant Z181100001718196. *(Xiaojing Shi and Zhe Zhang contributed equally to this work.) (Corresponding authors: Zhen Cheng; Zhenhua Hu; Jie Tian; Nan Ji.)*

Xiaojing Shi and Caiguang Cao are with the CAS Key Laboratory of Molecular Imaging, Beijing Key Laboratory of Molecular Imaging, The State Key Laboratory of Management and Control for Complex Systems, Institute of Automation, Chinese Academy of Sciences, China, and also with the School of Artificial Intelligence, University of Chinese Academy of Sciences, China.

Zhenhua Hu is with the CAS Key Laboratory of Molecular Imaging, Beijing Key Laboratory of Molecular Imaging, The State Key Laboratory of Management and Control for Complex Systems, Institute of Automation, Chinese Academy of Sciences, Beijing 100190, China, and also with the School of Artificial Intelligence, University of Chinese Academy of Sciences, Beijing 100049, China (e-mail: zhenhua.hu@ia.ac.cn).

Zhe Zhang is with the Department of Neurosurgery, Beijing Tiantan Hospital, Capital Medical University, China.

Zeyu Zhang is with the CAS Key Laboratory of Molecular Imaging, Beijing Key Laboratory of Molecular Imaging, The State Key Laboratory of Management and Control for Complex Systems, Institute of Automation, Chinese Academy of Sciences, China, and also with the Engineering Research Center of Molecular and Neuro Imaging of Ministry of Education, School of Life Science and Technology, Xidian University, China.

Zhen Cheng is with the Molecular Imaging Center, Shanghai Institute of Materia Medica, Chinese Academy of Sciences, Shanghai 201203, China (e-mail: zcheng@simm.ac.cn).

Jie Tian is with the CAS Key Laboratory of Molecular Imaging, Beijing Key Laboratory of Molecular Imaging, The State Key Laboratory of Management and Control for Complex Systems, Institute of Automation, Chinese Academy of Sciences, Beijing 100190, China, and with the School of Artificial Intelligence, University of Chinese Academy of Sciences, Beijing 100049, China, and with the Engineering Research Center of Molecular and Neuro Imaging of Ministry of Education, School of Life Science and Technology, Xidian University, Xi'an 710071, China, and also with the Beijing Advanced Innovation Center for Big Data-Based Precision Medicine, School of Medicine, Beihang University, Beijing 100191, China (e-mail: jie.tian@ia.ac.cn).

Nan Ji is with the Department of Neurosurgery, Beijing Tiantan Hospital, Capital Medical University, Beijing 100070, China, and with the Beijing Advanced Innovation Center for Big Data-Based Precision Medicine, School of Medicine, Beihang University, Beijing 100191, China, and also with the China National Clinical Research Center for Neurological Diseases, Beijing 100070, China (e-mail: jinan@bjtth.org).

This article has supplementary downloadable material available at https://doi.org/10.1109/TBME.2021.3130195, provided by the authors.

Digital Object Identifier 10.1109/TBME.2021.3130195

Abstract*—*Objective: **This translational study aims to investigate the clinical benefits of indocyanine green (ICG) based near-infrared window II (NIR-II) fluorescence image-guided surgery (FGS) on high-grade glioma (HGG) patients.** ***Methods:*** **Patients were randomly assigned to receive FGS or traditional white light image-guided surgery (WLS). The detection rate of NIR-II fluorescence was observed. Complete resection rate, progression-free survival (PFS), overall survival (OS), and neurological status were compared. Tissue samples were obtained from the FGS group, with the diagnosis based on the surgeons and the fluorescence recorded for comparison of diagnostic capability. Patients with WHO grade III gliomas or glioblastomas (GBM) were analyzed separately.** ***Results:*** **15 GBM and 4 WHO grade III glioma patients in the FGS group and 18 GBM and 4 WHO grade III glioma patients in the WLS group were enrolled. The detection rate of NIR-II fluorescence was 100% for GBM. The complete resection rate was significantly increased by the FGS for GBM (FGS, 100% [95% CI 73.41-100] *vs.* WLS, 50% [95% CI 29.03-70.97], $P = 0.0036$). The PFS and OS of the FGS group were also significantly prolonged (Median PFS: FGS, 9.0 months *vs.* WLS, 7.0 months, $P < 0.0001$; Median OS: FGS, 19.0 months *vs.* WLS, 15.5 months, $P = 0.0002$). No recurrence was observed in WHO grade III glioma patients.** ***Conclusions:*** **NIR-II FGS achieves a much better complete resection rate of GBM than conventional WLS, leading to greatly improved survival of GBM patients.** ***Significance:*** **NIR-II FGS is a highly promising technique worthy of exploring more clinical applications.**

***Index Terms*—Near-infrared window II, fluorescence image-guided surgery, glioblastoma, indocyanine green.**

I. Introduction

GLIOBLASTOMA (GBM) occurs as the most common primary tumor in the central nervous system [1]. The 5-year overall survival rate of GBM patients is only ~5% [2], [3]. Maximal safe resection is recommended as a beneficial approach to improve the overall survival (OS) and the progression-free

survival (PFS), benefiting the life quality of patients [4]–[6], which is strongly recommended for surgical decision by the European Society for Medical Oncology (ESMO) and National Comprehensive Cancer Network (NCCN) guideline of the central nervous system. However, maximal safe resection of GBM is hardly achieved because the GBM often infiltrates into the eloquent area. Besides, distinguishing the tumor from the non-tumor tissue in the resection margin even in the non-eloquent area is also difficult [7].

Several techniques including intraoperative ultrasound (iUS), intraoperative magnetic resonance imaging (iMRI), and neuro-navigation have been applied to assist neurosurgeons to achieve improved GBM resection during surgery [8]. Preoperative magnetic resonance imaging (MRI) based neuro-navigation can be affected by brain shift and deformation, reducing the accuracy of locating the tumor after craniotomy [9]. The iUS suffers limited resolution and is susceptible to interference from edema and bleeding during the resection, leading to poor judgment of the residual tumor. The iMRI is the only technique that improves the overall survival of glioma patients, but limitations such as inconvenience, time-consuming operation, and high cost restrict its' application in neurosurgery [10].

Therefore, a novel real-time imaging technique for precise intraoperative image-guided neurosurgery is urgently needed [11]–[16]. This demand has inspired the investigation of fluorescence image-guided surgery (FGS) techniques. For example, dyes emitting fluorescence in the visible wavelength (400-700 nm) such as 5-aminolevulinic acid (5-ALA) induced protoporphyrin IX (PpIX, $\lambda ex = 407$ nm, $\lambda em = 620$ nm) and fluorescein sodium (FS, $\lambda ex = 494$ nm, $\lambda em = 512$ nm) have been studied for real-time FGS, and they have improved the extent of resection (EOR) and PFS of high-grade glioma patients, including patients with GBM [17]–[20]. In 2006, a randomized controlled clinical trial demonstrated that 5-ALA based FGS has resulted in 65% of patients achieving complete resection of the tumor, while 36% of patients achieved complete resection in the white-light group [17]. 5-ALA based fluorescence imaging also has achieved a rather high positive-predictive value (PPV) in tumor detection, facilitating 5-ALA based FGS to be reliable to visualize the tumor [21]. As for FS, studies have proved that intraoperative bolus injection leads to its accumulation in areas with blood-brain barrier damage [22]. In a study of FS based FGS of high-grade gliomas implemented in 2018, 82.61% of the 46 patients involved achieved complete resection [20]. FS also has a higher sensitivity in identifying tumor tissues compared to 5-ALA [19]. However, the visible-light fluorescence has limitations such as poor tissue penetration and auto-fluorescence, which may decrease the contrast between the tumor and surrounding non-tumor tissue. Therefore, the near-infrared window I (NIR-I, 700-900 nm) fluorescence imaging has been investigated in gliomas resection surgery with FDA approved indocyanine green (ICG, $\lambda ex = 760$ nm, $\lambda em = 830$ nm). Previous clinical studies have demonstrated that ICG passes the disrupted blood-brain barrier and accumulates in GBM [23], rendering it a promising optical probe for intraoperative imaging of GBM. Moreover, ICG injected at a higher dose and 24 hours ahead of imaging can achieve even higher sensitivity and negative-predictive value (NPV), which enables surgeons to find more residual tumors [24].

Recently, near-infrared window II (NIR-II, 1,000-1,700 nm) fluorescence imaging has been demonstrated to possess significant advantages in biological imaging compared with the conventional NIR-I fluorescence imaging in recent studies. Low autofluorescence of tissue in the NIR-II spectrum enables accurate *in vivo* detection of the fluorophore. Furthermore, the low tissue absorption and scattering property of NIR-II light provide a high contrast image of deeper tissue compared with fluorescence imaging in NIR-I and visible spectrum. The outstanding optical imaging properties of NIR-II fluorescence have led to outstanding performance of NIR-II imaging in broad of preclinical applications [25], [26]. Although numerous studies confirm that NIR-II out-performs NIR-I fluorescence imaging in pre-clinical studies using small animal models, research on the clinical application of NIR-II imaging is rare and in infancy, which is mainly attributed to the lack of clinical approved imaging instruments and molecular probes. More importantly, until now there is no report to investigate the clinical impact and treatment efficacy of NIR-II image-guided surgery. In recent years, ICG was reported to have fluorescence in the NIR-II region in addition to the emission peak in the NIR-I region. This facilitated a fast clinical translation of NIR-II fluorescence imaging [25]. The first clinical application of NIR-II fluorescence imaging was reported using ICG in a group of hepatocellular carcinoma patients and proved a better imaging performance of NIR-II compared with NIR-I [26].

Herein, we have developed and characterized a novel multispectral imaging system (visible/NIR-I/NIR-II) suitable for intraoperative brain tumor imaging. Then a randomized control clinical trial has been conducted to evaluate medical value and treatment efficacy of NIR-II image-guided surgery. More specifically, GBM patients were randomly assigned as FGS group or white light image-guided surgery (WLS) group. The outcome of the surgery such as detection rate, complete resection rate, PFS, OS, and neurological function of GBM patients have been analyzed. The medical value and benefits of NIR-II FGS have been clearly demonstrated by comparison with conventional surgery under white light which is the current standard clinical practice.

II. Materials and Methods

A. Construction of Intraoperative Brain Tumor Multispectral Imaging System

To perform NIR-II FGS of gliomas, a novel multispectral imaging system was developed, which can acquire color (400-700 nm), NIR-I (700-900 nm), and NIR-II (1,000-1,700 nm) images intraoperatively. The imaging system was composed of an imaging sub-system and a controlling sub-system. The imaging sub-system was used to achieve the color image and NIR-II/I fluorescence images, which consisted of a laser generation unit, a visible light imaging unit, a NIR-I imaging unit, and a NIR-II imaging unit. The NIR-II imaging unit contained a camera (NIRvana: 640, Teledyne Princeton Instruments, USA) using InGaAs imaging chip, a lens specially

designed for shortwave-wavelength infrared imaging with a high performance (SWIRON 2.8/50, Schneider Kreuznach, Germany), and a long-pass filter (over 1000 nm, FEL1000 Longpass Filter, Thorlabs, USA). The NIR-I imaging unit included an electron-multiplying charge-coupled device (EMCCD, ProEM-HS: 1024BX3, Teledyne Princeton Instruments, USA), a lens (VHF 35M-MP SWIR, Spacecom, Japan), and a spectral filter (over 850 nm, FEL0850 Longpass Filter, Thorlabs, USA). A mobile phone (Huawei Enjoy 9, Huawei, China) was connected with the controlling unit to serve as the visible light imaging unit. The laser generation unit is composed of an 808 nm laser, a liquid-core optical fiber, and a collimator. The collimator converted the concentrated light beam into a dispersed and homogenize light spot. The power of the laser was set to be 50 mW/cm^2. The controlling sub-system which included a laser distance measurement unit, a controlling handle, and a computer was set to control the imaging subsystem to rotate so that images of every side of the tumor cavity were acquired.

A specialized program was realized using MATLAB (MATLAB R2018b, The MathWorks Inc., USA) to convert the fluorescence image from a grayscale image to a pseudocolor image. A threshold was assigned intraoperatively to indicate the signal intensity of tumors. Pixels with signal intensity below the threshold were displayed with no pseudo color to indicate normal tissue, while pixels with signal intensity above the threshold were assigned a color from the gradient region of yellow and blue to indicate tumor tissue. The color of pixels with higher signal intensity was closer to yellow, while the color of pixels with signal intensity closer to the threshold was closer to blue.

The multispectral imaging system was 160 cm in the length, and 60 cm in the width. The height of the imaging system was adjustable, ranging from 140 to 190 cm. This guaranteed the changeable imaging distance.

B. Patients' Characteristics

Patients matching the following criteria were enrolled: (1) patients aged 18-75 years with suspected newly diagnosed, untreated gliomas, who were eligible for surgical resection; (2) patients with KPS over 70; (3) patients with only one solid contrast-enhanced lesion on MRI before randomization, which is not located in the midline, basal ganglia, cerebellum, or brain stem of the brain; (4) patients with normal heart, bone marrow, liver, and kidney function, which are determined by laboratory tests before surgery (ie. hemoglobin $>$110g/L, platelet count $>100\times10^9$, total bilirubin level $<$ 1.5 $\times$ upper limit of normal (ULN), alanine aminotransferase/glutagory aminotransferase $<$ 2.5 $\times$ ULN; creatinine $<$ 1.5 $\times$ ULN); (5) patients who are compatible with follow-up; (6) women of child-bearing age receiving a pregnancy test within 7 days before initiation of treatment with negative results; (7) male and female patients with fertility agreeing to use effective contraceptive measures to ensure no pregnancy during the study period and within 3 months after discontinuation of treatment; (8) patients volunteered to sign the informed consent form; (9) patients have complete medical records for analysis. Exclusion criteria were as follows: (1) patients who are unable to sign the informed consent form; (2) patients with gliomas that are not suitable for resection; (3) patients allergic to ICG; (4) patients with any unstable systemic disease (including active infections, uncontrolled hypertension, unstable angina, angina pectoris within the last 3 months, congestive heart failure, occurred within 12 months of enrollment myocardial infarction, severe arrhythmia requiring medication, liver, kidney or metabolic disease); (5) patients who are infected with human immunodeficiency virus (HIV) or with active hepatitis; (6) patients who have participated in other clinical trials within the past 30 days; (7) patients with mental illness, cognitive impairment, who are unable to understand the experimental scheme and side effects and to complete the experimental arrangements and follow-up. The patients enrolled were randomly allocated to the FGS group or the WLS group.

Assuming that the complete resection rate of the FGS group and WLS group are 85% and 40% respectively, the sample size of each group was required to be 15 ($\alpha = 0.05$, two-sided type, and power ($1 - \beta$) of 80%. Sample size ratio is 1:1). With a maximum of 30% incomplete follow-up or dropout expected, 20 patients were planned to be involved in each of the groups.

The protocol was authorized by the Ethics Committee of Beijing Tiantan Hospital, Capital Medical University. The clinical trial was registered in the Chinese Clinical Trial Registry (ChiCTR2000029402). From March 22 to August 23, 2019, 40 GBM patients were enrolled. All patients were given informed consent for their agreements. Patients were randomly allocated to the FGS group (n = 20) and the WLS group (n = 20). In the FGS group, 5 patients were excluded for withdrawing consent before surgery (n = 2), not meeting histopathological criteria after surgery (n = 1), and not receiving standard treatment (n = 2). In the WLS group, 2 patients were excluded for missing radiological data of postoperative MRI (n = 1) and not meeting the histopathological criteria after surgery (n = 1). In the end, 15 patients in the FGS group and 18 in the WLS group met the inclusion criteria of this trial (Fig. 1(a)). All the patients in both of the groups received Stupp standard treatment after surgery.

Eight patients with WHO grade III patients were also enrolled and analyzed separately.

C. Study Design

Patients all went through MRI examination before surgery. For the patients assigned to the FGS group, ICG (1mg/kg) was injected intravenously 48 hours before intraoperative fluorescence imaging. NIR-II/I fluorescence images of tumor was acquired intraoperatively and the NIR-II fluorescence images were shown to the surgeons to guide the tumor resection under the microscope. Tissue samples were obtained for *ex vivo* fluorescence imaging and histopathological analysis. For the patients in the WLS group, placebo was not employed. And the tumor was resected under the microscope in a conventional manner. The grade of each patient in both of the group was determined by pathological analysis of tumor tissue sample after surgery (Fig. 1(b)).

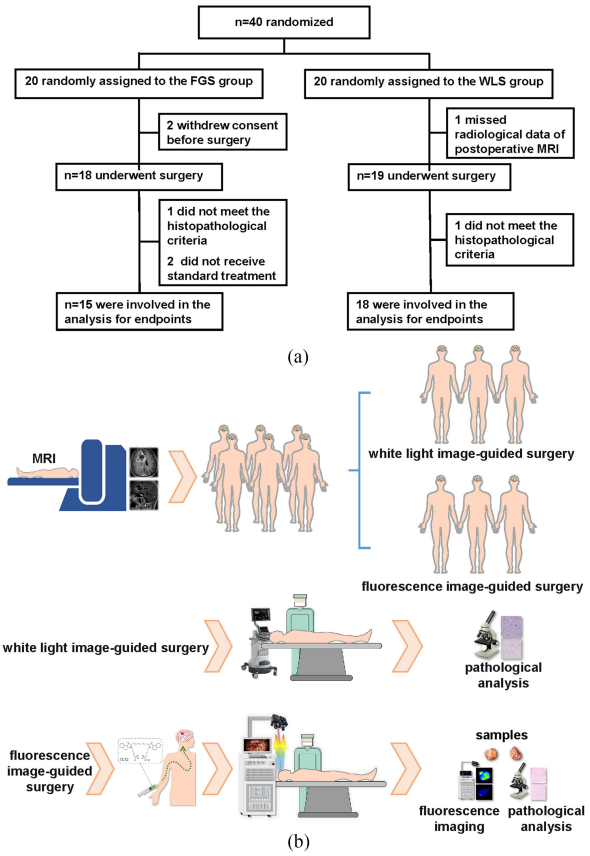

Fig. 1. Clinical trial profile. The patient enrollment process (a), and the schematic diagram of the trial (b), were displayed above.

D. Intraoperative NIR-II/I Fluorescence Imaging of GBM and Surgery Under the Guidance of NIR-II Fluorescence Images

The intraoperative brain tumor imaging system was sterilely draped before utilization in the operating room. At the beginning of the surgery, the neuro-navigation based on preoperative MRI was applied only for determining the position of the incision. Upon opening of the dura and the exposure of the cortex, the imaging system was positioned near the operation bed and the working distance was adjusted to 50 cm. Color images were acquired under the light in the operating room. Then the light was turned off and NIR-II/I fluorescence images were acquired with the exposure time ranging from 500 to 2000 ms. The presence or absence of NIR-II/I fluorescence was recorded for each patient. The detection rate of the fluorescence was calculated as follows: detection rate = number of patients with tumor fluorescence/number of patients involved in the FGS group. For patients with the fluorescence of tumors, the resection extent was displayed by the NIR-II fluorescence images. The gross tumor was removed by the surgeons under the microscope referring to the NIR-II fluorescence images. After the surgeon was satisfied with the resection, color images and NIR-II/I fluorescence images were acquired again to prompt whether the tumor tissue was left. Tissue with residual NIR-II fluorescence signal was removed with the consideration of the neurological function reservation.

E. Ex Vivo NIR-II/I Fluorescence Imaging of Tissue Samples

Tissue samples with a side length of about 1 cm were obtained from the gross tumor and the tissues with residual NIR-II fluorescence. Color and NIR-II/I fluorescence images of the samples set on black cardboard were obtained using our imaging system in the operating room.

F. Diagnosis of Tissue Samples Based on the Fluorescence Images and Surgeons in the Operating Room

The samples were coded whether they were tumor tissue or normal tissue by three surgeons who were blind to the fluorescence images while still in the operating room. In the meantime, the existence or absence of NIR-II/I fluorescence in the fluorescence images of each sample was coded by another surgeon, with the existence of fluorescence marked as tumor and absence of fluorescence as non-tumor tissue. The diagnosis based on the surgeons and fluorescence was then compared with the histopathological diagnosis of the samples obtained after the surgery, which served as the gold standard.

G. Endpoints

The primary endpoint was the proportion of patients without residual tumors measured on post-operative MRI. The secondary endpoints were the PFS 6 months and neurological function 3 months after surgery.

To evaluate the proportion of patients without residual tumor, the complete resection rate was introduced and calculated as follows: complete resection rate = the number of patients with complete resection of tumor / the number of patients in each group. Complete resection was defined as enhancement on T1-enhanced MRI with a volume of less than 0.175 cm^2 measured from the postoperative MRI obtained within 72 hours after the surgery.

The patients were followed up every 3 months to assess disease progression. Progression was defined according to the Response Assessment in Neuro-Oncology (RANO) criteria. PFS at 3, 6, 9, and 12 months were calculated as the proportion of patients without progression at a certain time. For example, PFS at 6 months after surgery (6m-PFS) = number of patients that don't have progress at 6 months after surgery/number of patients involved. When comparing the PFS, the impact of age, sex, neurological function, EOR, IDH, 1p19q, and MGMT promoter methylation was eliminated through calibration.

To analyze the neurological function, patients were divided into three groups according to the level of GBM infiltration to the eloquent area. Tumors located in non-eloquent areas were defined as eloquent grade I. Eloquent grade II tumors included the tumors located near eloquent brain areas. Eloquent grade III tumors referred to those involving the eloquent brain areas.

As the indexes of neurological function, general physical performance and neurologic status were evaluated by KPS and the NIHSS respectively. Preoperative (pre-op) evaluation was performed within 7 days before surgery, and postoperative (post-op) evaluation was completed within 72 hours after surgery (imm. post-op) and 3 months after surgery (3m. post-op).

H. Pre- and Post-Operative MRI

The preoperative MRI was performed within 7 days before surgery and postoperative MRI within 72 hours and every 3 months after surgery with Dimeglumine Gadopentetate Injection (0.1 mmol/kg, Beijing Beilu Pharmaceutical Co., Ltd., China) injected intravenously. All the MRI was performed using a 3.0T General Electric clinical scanner (Discovery MR750, General Electric Company, USA) and each slice was 6 mm thick. Contrast-enhanced T1-weighted (T1W) sequences were used for volumetric analysis.

I. Histopathologic and Molecular Analysis

The histopathological grade of all the tissue samples was classified by three neuropathologists who were masked to the study based on the 2016 World Health Organization (WHO) Classification of Tumors of the Central Nervous System.

To evaluate the Ki-67 index of samples, immunohistochemistry staining was performed to the sample. Slices of tissue microarray sections were scanned using a digital whole slide scanner at 400× magnification (Aperio AT2, Leica, Germany). The expression of Ki-67 were analyzed using the Aperio ImageScope (12.3.0.5056, Leica, Germany). For each tissue section, counting of Ki-67 immunoreactive cells and nonreactive cells were performed on the whole section. The Ki-67 index = the number of Ki-67 positive cells / (the number of Ki-67 positive cells + the number of Ki-67 negative cells).

Molecular detection of IDH status, 1p19q codeletion, and MGMT promoter methylation were recorded according to Electronic Medical Record.

J. Image Analysis

The tumor volumes were calculated using MRIcron software (www.nitrc.org). The tumor was manually segmented on each slice of MRI, with the volume on each slice calculated by the software. The total tumor volume was the accumulation of volume on each slice. All tumor volumes were evaluated by three neuro-radiologists who were blinded to the patients' clinical information. The EOR = (preoperative tumor volume – postoperative tumor volume) / preoperative tumor volume ×100%.

The region of interest analysis using ImageJ (National Institute of Health, USA) was applied to quantitatively measure the NIR-II/I fluorescence intensity. The tumor-to-normal tissue ratio (TNR) of the *in vivo* fluorescence images and the signal-to-background ratio (SBR) of the *ex vivo* fluorescence images were calculated as follow: TNR = mean signal intensity of the tumor region / mean signal intensity of the normal tissue region; SBR = mean signal intensity of the tumor sample region / mean signal intensity of the blackboard region.

K. Statistical Analysis

The quantitative data included the TNR of intraoperative NIR-II/I fluorescence images and the SBR of fluorescence images of the tumor tissues and non-tumor tissues. Quantitative data were presented as mean ± s.d.. A two-sided Mann-Whitney U-test was employed for data comparisons between two groups. To evaluate the difference among the pre- and post-operative (imm. and 3m. post-op) NIHSS and KPS, Kruskal-Wallis tests, and Dunn's multiple comparisons were applied. Spearman's correlation analysis and Pearson's correlation analysis were applied to evaluate the correlations between the SBR and the WHO grade as well as the Ki-67 index of the samples respectively. Clinical characteristics, including sensitivity, specificity, NPV, PPV, and accuracy between two groups (NIR-II and surgeon; NIR-II and NIR-I), were compared using the Chi-square test and Fisher exact test. The log-rank test was performed to assess PFS based on prognostic factors between the two groups.

III. Results

A. The Intraoperative Brain Tumor Multispectral Imaging System

To perform NIR-II FGS for patients with gliomas, an intraoperative brain tumor multispectral imaging system was first constructed, which was capable of NIR-I, NIR-II, and color imaging, and was composed of two sub-systems for imaging and controlling (Fig. 2(a)). The key parameters of the system were determined and are listed in Table I. The system can be easily placed in the neurosurgical operating room (Fig. 2(b)) and conveniently used by neurosurgeons. For the FGS group, the neurosurgeons depended on the NIR-II fluorescence images to guide the resection (Fig. 2(c)).

B. Verification of the NIR-II/I Imaging System and Tumor Resection Method Under the Guidance of NIR-II Images Using Phantoms and Tumor-Bearing Mice

The imaging system was first verified by the phantom study. The NIR-II/I fluorescence intensity acquired by the system had a linear correlation with the ICG concentration (Fig. 2(d)), with correlation equations to be $Y = 0.26 \times X + 0.18$ ($R^2 = 0.96$) for NIR-II and $Y = 0.87 \times X - 0.40$ ($R^2 = 0.97$) for NIR-I (Fig. 2(e)). More importantly, NIR-II fluorescence imaging achieved much higher SBR compared with NIR-I. For ICG with a concentration of 1.5×10^{-3} mg/ml, SBR of 86.70 ± 5.78 for NIR-II *vs.* 37.75 ± 1.93 for NIR-I were obtained (Fig. 2(f)).

Phantom imaging study demonstrated that both NIR-I and NIR-II imaging can differentiate the four capillaries filled with ICG solution with no intralipid covered on them (Fig. S1A, row 1). When the capillaries were submerged 2 mm and 5 mm below the surface of the intralipid, the four capillaries were still distinguished by NIR-II/I imaging (Fig. S1(a), row 2, and 3). But when the capillaries were submerged 7 mm below the

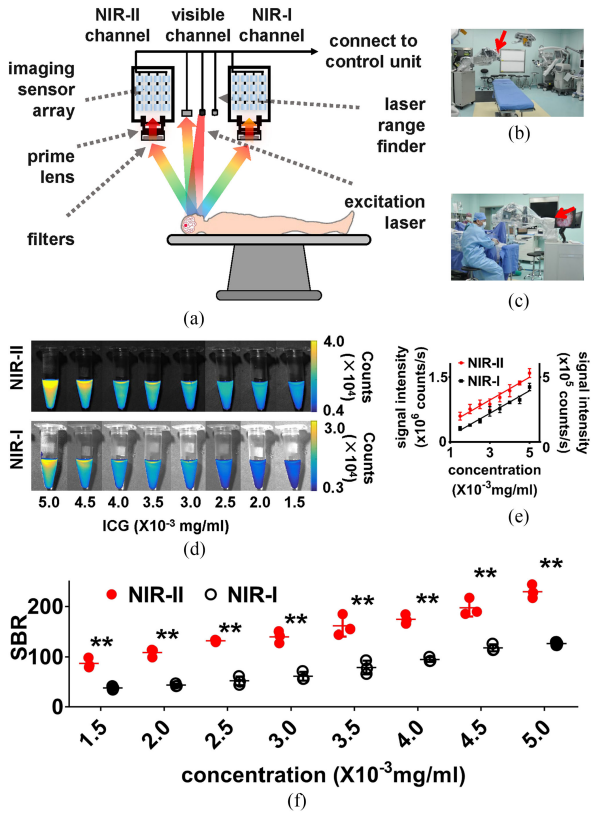

Fig. 2. The description of the multispectral fluorescence imaging system. (a), The schematic diagram of the multispectral fluorescence imaging instrument. (b), and (c), the instrument (pointed out by the red arrow) placed in the operating room and used in NIR-II fluorescence image-guided surgery. (d), NIR-II/I fluorescence images of ICG dissolved in FBS of different concentrations. (e), the correlation function between the fluorescence intensity and the concentrations were $Y = 0.26 \times X + 0.18$ for NIR-II and $Y = 0.87 \times X - 0.40$ for NIR-I. (f), NIR-II fluorescence imaging has a significantly higher SBR than NIR-I. The minimum concentration of ICG in FBS that can be detected by the instrument was 64.5 fM (5×10^{-11}mg/ml) for NIR-II and 3.22 fM (2.5×10^{-12}mg/ml) for NIR-I.

surface, it became difficult to distinguish the 2 capillaries with the distance of 5 mm using both NIR-II and NIR-I imaging, but the 2 capillaries with the distance of 10 mm were still distinguished on the fluorescent images (Fig. S1(a), row 4). When the capillaries were submerged 12 mm below the surface, the 2 capillaries with a distance of 10 mm were not distinguished (Fig. S1(a), row 5). The quantitative plot of intensity across a line of interest showed a higher contrast of NIR-II than NIR-I to distinguish the capillary from the background signal (Fig. S1(a), column 3, and 5).

Both NIR-II and I fluorescence imaging of orthotopic U87MG tumor-bearing mice showed that ICG can accumulate in the GBM with good contrast. The fluorescence of the tumor was visualized even without opening the scalp (Fig. S1(b), column 1), and the tumor became more obvious upon opening the skull (Fig. S1(b), column 2). Then the tumor was removed under the guidance of the NIR-II fluorescence images (Fig. S1(b), column 3, and 4). Quantitative data of the images showed that the TNR of both NIR-II and NIR-I dropped dramatically after the removal of the tumor (Fig. S1(c)).

TABLE I
KEY PARAMETERS FOR THE INTRAOPERATIVE BRAIN TUMOR MULTISPECTRAL IMAGING SYSTEM CONSTRUCTED

Instrument features	Parameters
Imaging channels	NIR-II, NIR-I
Device type	NIRvana: 640, Teledyne Princeton Instruments (NIR-II) ProEM-HS: 1024BX3, Teledyne Princeton Instruments (NIR-I)
Chip image area (mm×mm)	12.80×10.24 13.30×13.30
Highest temporal resolution (ms)	45.45 (NIR-II) 33.33 (NIR-I)
Working distance (cm)	50
Surgical field of view (cm× cm)	10.66×8.53 17.07×17.07
Sensor resolution (imaging pixels)	640×512 1024×1024
Imaging resolution (μm)	62.5 (NIR-II) 92 (NIR-I)
Sensitivity (ICG, fM)	64.50 (NIR-II) 3.22 (NIR-I)
Optical filter	1000 nm long pass, FEL 1000, Thorlabs (NIR II) 850 nm long pass, FEL0850, Thorlabs (NIR-I)
Laser fiber	liquid core optical fiber
Beam expander	Customized, made of a spherical glass Beam divergence 18 mrad
Image windows	NIR-II; NIR I; Visible (Color); Overlay

C. Intraoperative NIR-II/I Fluorescence Imaging and Surgery Under the Guidance of NIR-II Fluorescence Images

For a participant with GBM, the preoperative T1-enhanced MRI exhibited enhancement in the left frontal-parietal lobe as pointed out by the red arrows (Fig. 3(a), left, labeled as pre-op). The postoperative MRI displayed no enhancement, which indicated total resection of the tumor (Fig. 3(a), right, labeled as post-op). After removing the bone flap and the dura, the color image and NIR-II/I fluorescence images were acquired above the cortex. The extent of resection can be displayed by the fluorescence images (Fig. 3(b), row 1, labeled as pre-op). The surgeons then removed the gross tumor under the assistance of a microscope referring to the NIR-II fluorescence image. After the surgeon declared that the tumor was totally resected, the NIR-II/I fluorescence images were acquired again, which displayed no residual NIR-II/I fluorescence (Fig. 3(b), row 2, labeled as post-op). Quantitative analysis showed that TNR of NIR-II were significantly higher than that of NIR-I (NIR-II 6.50 $\pm$ 3.45 *vs.* NIR-I 4.04 $\pm$ 2.20, $P = 0.0230$), which sharply dropped after the resection (NIR-II, before resection 6.50 $\pm$ 3.45 *vs.* after resection 1.05 $\pm$ 0.22, $P < 0.0001$; NIR-I, before resection 4.04 $\pm$ 2.20 *vs.* after resection 1.07 $\pm$ 0.13, $P < 0.0001$, Fig. 3(c)). *Ex vivo* images of tissue samples obtained from the tumor were acquired during the surgery (Fig. 3(d), column 1). The tissue samples displayed NIR-II/I fluorescence (Fig. 3(d), column 2 and 3), with further histopathological diagnosis demonstrated the samples to be tumor tissue (Fig. 3(d), column 4).

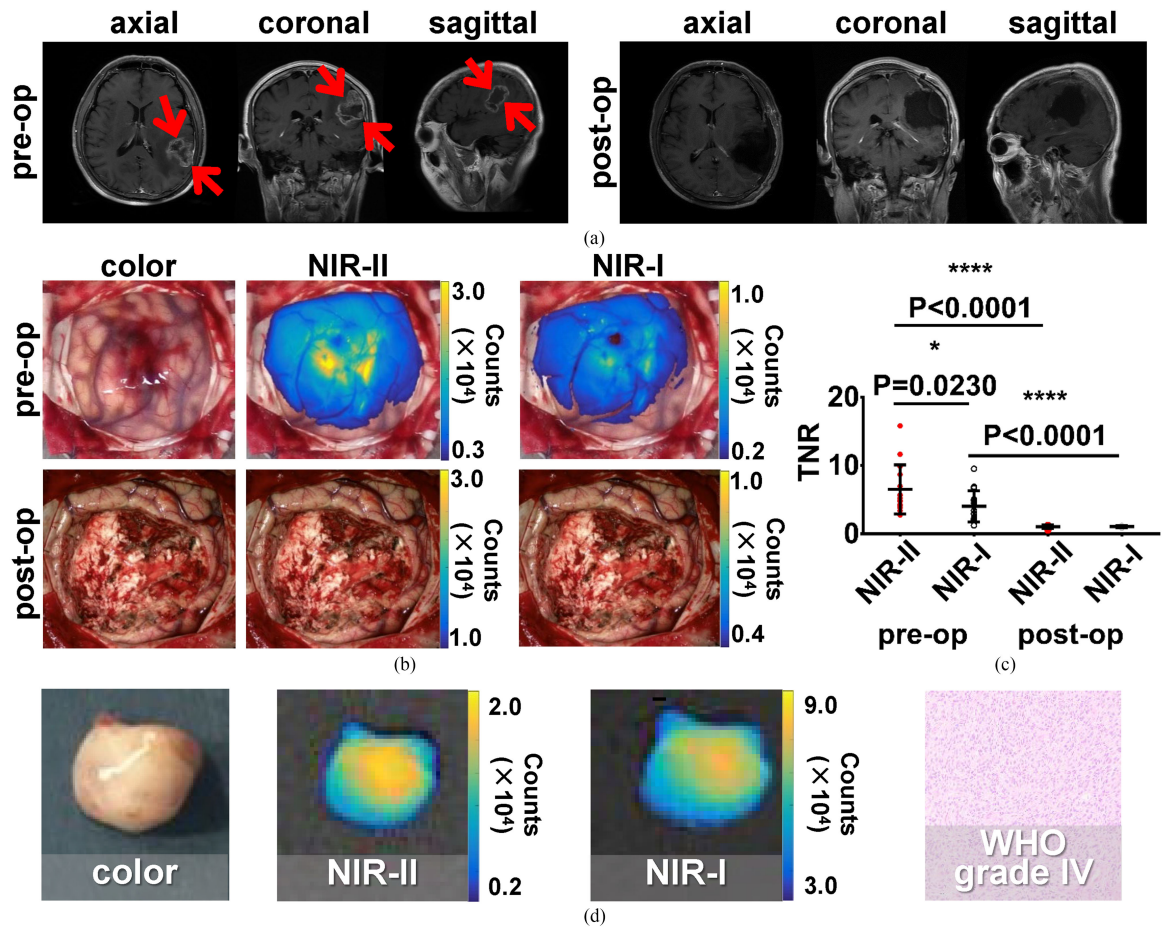

Fig. 3. A typical patient with glioblastoma showing obvious tumor fluorescence intraoperatively. (a), the pre-operative T1-enhanced MRI demonstrated enhancement in left frontal-parietal lobe (left), and the post-operative T1-enhanced MRI displayed no residual enhancement (right). (b), the color and NIR-II or NIR-I fluorescence images were acquired upon the opening of the dura, and after all the tissue with NIR-II fluorescence signal was removed. (c), the TNR of NIR-II or NIR-I decreased sharply after resection. (d), the tissue sample obtained from the tumor (column 1) was imaged *ex vivo* after surgery and showed obvious NIR-II or NIR-I fluorescence (column 2 and 3). Post-operative histopathology images confirmed that the sample was tumor tissue (column 4).

D. Ex Vivo Fluorescence Imaging and Diagnosis of the Samples

A total of 235 tissue samples were obtained from the 15 patients who underwent FGS, including 154 tumor tissue samples (65.53%) and 81 non-tumor tissue samples (34.47%) according to the histopathological diagnosis. Tumor tissue samples, classified into 3 grades (WHO grade II, III, and IV) according to the histopathology, displayed obvious NIR-II/I fluorescence (Fig. 4(b)–(d)), while non-tumor tissue samples displayed no obvious fluorescence (Fig. 4(a)). The SBR of NIR-II fluorescence imaging was significantly higher compared with NIR-I ($P = 0.0070$, Fig. 4(e)). With the analysis of the SBR of the tumor and non-tumor tissue, it is proved that the tumor had a significantly higher SBR than non-tumor tissue for both NIR-II and I (NIR-II $P < 0.0001$, NIR-I $P < 0.0001$, Fig. 4(f)). This indicated the feasibility of using SBR obtained from *ex vivo* tissue imaging as a diagnostic indicator to distinguish tumor from non-tumor tissue. Therefore, the receiver operating characteristic (ROC) curves were obtained to compare the diagnostic accuracy of NIR-II or NIR-I imaging and the surgeons' diagnosis. The area under curve (AUC) of the NIR-II or NIR-I imaging was significantly larger than that of surgeon's diagnosis (NIR-II 0.9997 [95% CI 0.9989 - 1.0000] *vs.* surgeons' diagnosis 0.8009 [95% CI 0.7384 - 0.8634], difference between groups 0.1988, $P < 0.0001$; NIR-I 0.9899 [95% CI 0.9813 - 0.9986] *vs.* surgeons' diagnosis 0.8009 [95% CI 0.7384 - 0.8634], difference between groups 0.1890, $P < 0.0001$, Fig. 4(g), Tables II and III). Compared with NIR-I fluorescence imaging, the AUC of NIR-II imaging was also significantly higher (NIR-II 0.9997 [95% CI 0.9989 - 1.0000] *vs.* NIR-I 0.9899 [95% CI 0.9813 - 0.9986], difference between groups 0.0098, $P = 0.0204$, Fig. 4(g)). This result suggested that NIR-II had the highest diagnostic capability, followed by NIR-I and surgeon's intraoperative diagnosis (Fig. 4(g)).

To further compare the diagnostic ability of NIR-II/I fluorescence imaging and surgeons' diagnosis, the indexes such as sensitivity, specificity, PPV, NPV, and diagnostic accuracy were calculated (Table III). The NIR-II had significantly higher sensitivity, specificity, PPV, NPV, and accuracy compared with surgeons' diagnoses (sensitivity, NIR-II: 100% [95% CI 97.07

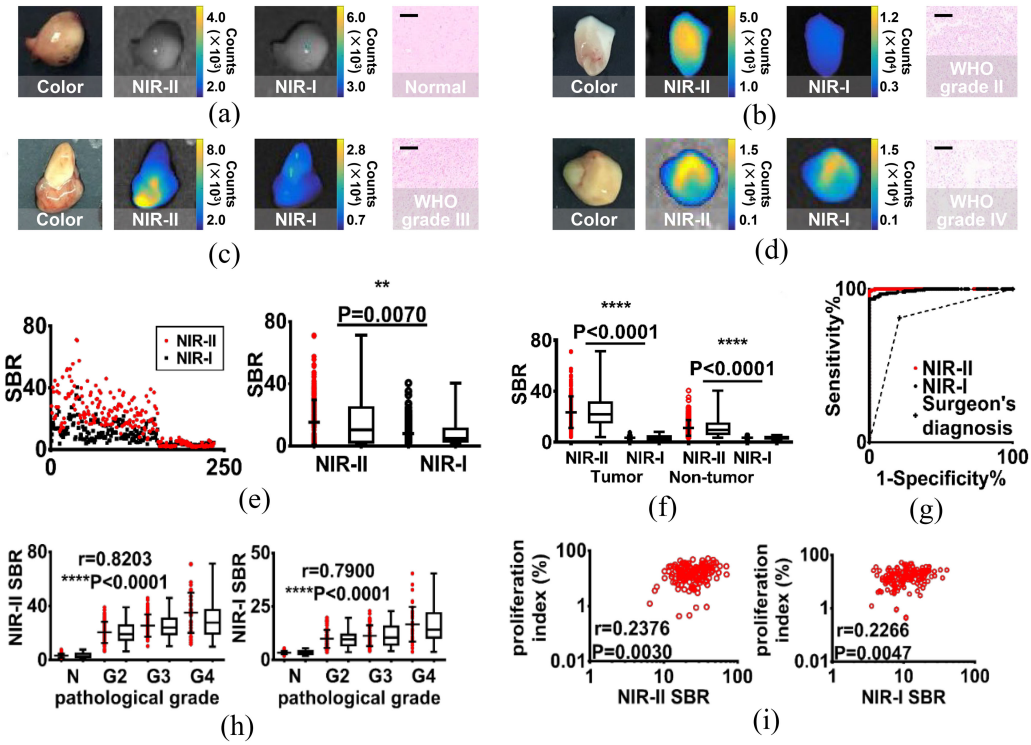

Fig. 4. Fluorescence images of samples. (a), A non-tumor tissue showed no obvious fluorescence of NIR-II and NIR-I, while tumor tissues of WHO grade II (b), WHO grade III (c), and WHO grade IV (d) showed obvious fluorescence. The histopathology images were displayed at 400 times magnified, and the black scale chart represented 50 μm. (e), SBR of the NIR-II or NIR-I fluorescence images of the 235 samples were plotted (left) and compared (right). (f), significant differences were found between the SBR of tumor samples (n=154) and non-tumor samples (n=81) for both NIR-II ($P < 0.0001$) and NIR-I ($P < 0.0001$). (g), the ROC of NIR-II/I SBR and surgeon's diagnosis was plotted. (h), SBR of samples was correlated with varying WHO grades (NIR-II, r = 0.8203, $P < 0.0001$ *vs.* NIR-I, r = 0.7900, $P < 0.0001$). (i), scatter plot of log SBR *vs.* log proliferation index showed a correlation between them (NIR-II, r = 0.2376, $P = 0.0030$ *vs.* NIR-I, r = 0.2266, $P = 0.0047$).

TABLE II
BASELINE CHARACTERISTICS

Variables	FGS (n = 15)	WLS (n = 18)	P-value
Age (Mean, years)	51.73±11.24	53.83±14.73	0.6540
Sex (Male/Female)	7/8	12/6	0.6428
Pre-op KPS (Median, range)	90(70-90)	90(70-100)	0.8725
Pre-op NIHSS (Median, range)	1(1-2)	1(0-2)	0.4210
Pre-op TV (cm^3, Mean)	64.94±25.47	49.53±35.26	0.6295
IDH			1.0000
mutation	1	2	
wild-type	14	16	
1p/19q co-deletion	0	0	-
MGMT			0.7970
methylation	6	8	
unmethylation	9	10	
Eloquence			
Grade I/II/III	4/7/4	4/7/7	0.7347
detection rate (%)	100.00	-	-
complete resection rate (%)	100.00	50.00	0.0036
6m-PFS	100.00	66.67	0.0134
	NIR-II fluorescence diagnosis	**Surgeons' diagnosis**	***P*-value**
Sensitivity (%)	100.00	81.17	$P < 0.0001$
Specificity (%)	91.36	79.01	0.0449
PPV (%)	95.65	88.03	0.0182
NPV (%)	100.00	68.82	$P < 0.0001$
Accuracy (%)	97.02	80.51	$P < 0.0001$

FGS, fluorescence image-guided surgery; WLS, white light image-guided surgery; KPS, Karnofsky performance score; NIHSS, National Institutes of Health Stroke Scale; TV, tumor volume; PFS, progression-free survival; NPV, negative-predictive value; AUC, area under the curve.

TABLE III
CHARACTERISTIC TESTS OF SPECIMENS

Surgeons' diagnosis		Histopathology									
		T	N			sensitivity	specificity	PPV	NPV	accuracy	AUC
Surgeon's diagnosis	T	125	17	142	Point estimate	81.17	79.01	88.03	68.82	80.51	0.8009
	N	29	64	93	(95% CI)	(74.22-86.60)	(68.84-86.56)	(81.57-92.48)	(58.79-77.36)	(74.96-85.08)	(0.7384-0.8634)
Total		154	81								
NIR-II SBR		Histopathology									
		T	N								
Fluorescence diagnosis	T	154	7	161	Point estimate	100.00	91.36	95.65	100.00	97.02	0.9997
	N	0	74	74	(95% CI)	(97.07-100.00)	(82.96-96.01)	(91.13-98.04)	(94.09-100.00)	(93.86-98.67)	(0.9989-1.0000)
Total		154	81								
NIR-I SBR		Histopathology									
		T	N								
Fluorescence diagnosis	T	150	15	165	Point estimate	97.40	81.48	90.91	81.48	91.91	0.9899
	N	4	66	70	(95% CI)	(93.28-99.21)	(71.55-88.56)	(85.45-94.51)	(71.55-88.56)	(87.66-88.56)	(0.9813-0.9986)
Total		154	81								

SBR, signal-to-background ratio; PPV, positive predictive value; NPV, negative predictive value; AUC, Area Under Curve.

- 100.00] *vs.* Surgeons: 81.17% [95% CI 74.22 - 86.60], difference between groups 18.83%, $P < 0.0001$; specificity, NIR-II: 91.36% [95% CI 82.96 - 96.01] *vs.* Surgeons: 79.01% [95% CI 68.84 - 86.56], difference between groups 12.35%, $P = 0.0449$; PPV, NIR-II: 95.65% [95% CI 91.13 - 98.04] *vs.* Surgeons: 88.03% [95% CI 81.57 - 92.48], difference between groups 7.62%, $P = 0.0182$; NPV, NIR-II: 100% [95% CI 94.09 - 100.00] *vs.* Surgeons, 68.82% [95% CI 58.79 - 77.36], difference between groups 31.18%, $P < 0.0001$; accuracy, NIR-II: 97.02 [95% CI 93.86 - 98.67] *vs.* Surgeons: 80.51% [95% CI 74.96 - 85.08], difference between groups 16.51%, $P < 0.0001$. Tables II and III). Besides, the diagnostic accuracy of the NIR-II fluorescence imaging was also significantly higher than that of NIR-I fluorescence imaging (Tables II and III).

Further investigation indicated a stronger correlation between SBR of NIR-II and the WHO grade of tissue samples compared with NIR-I (correlation coefficient: NIR-II 0.8203, $P < 0.0001$ *vs.* NIR-I 0.7900, $P < 0.0001$, Fig. 4(h)). The correlation between the SBR and proliferation index represented by the percentage of Ki-67 positive cells was also investigated (NIR-II, $r = 0.2376$, $P = 0.0030$ *vs.* NIR-I, $r = 0.2266$, $P = 0.0047$, Fig. 4(i)).

E. Detection Rate, Complete Resection Rate, PFS, and Neurological Function of GBM Patients

The detection rate of the NIR-II fluorescence imaging in this trial is 100%, with all the 15 glioblastoma patients showing obvious tumor fluorescence intraoperatively.

Patients underwent FGS showed significantly higher tumor complete resection rate compared to those underwent routine white-light surgery (100% [13/13, 95% CI 73.41-100] *vs.* 50% [9/18, 95% CI 29.03-70.97], $P = 0.0036$, Table II). In the 15 patients who underwent FGS, two patients had residual fluorescence signal intraoperatively, with confirmation by the surgeon that the fluorescence signal infiltrated to the eloquent areas and complete resection could not be realized considering the protection of neurological function. Postoperative enhanced MRI confirmed that the 2 patients had residual tumor tissue. For the other 13 patients with total removal of fluorescent tissue, no residual tumor tissue was observed in postoperative MRI.

The PFS and OS of the FGS group were remarkably prolonged compared with the WLS group (PFS, $P < 0.0001$, Fig. 5(a); OS, $P = 0.0002$, Fig. 5(b)). Median PFS was 9.0 months for the FGS group and 7.0 months for the WLS group. Median OS of 19.0 months and 15.5 months were achieved by FGS and WLS groups. Importantly, PFS at 6 months for patients in FGS group was significantly higher than WLS group (100% [15/15, 95% CI 76.14-100.00] *vs.* 66.67% [12/18, 95% CI 43.57-83.90], $P = 0.0134$, Table II).

F. Detection Rate, Complete Resection Rate, PFS, and Neurological Function of WHO Grade III Glioma Patients

In addition to GBM patients, the performance of intraoperative NIR-II fluorescence imaging was also evaluated in patients with grade III gliomas. Eight patients were involved and randomly assigned to the WLS or FGS groups. Fluorescence of tumor was observed in 3 of the 4 patients in the FGS group, leading to a detection rate of 75%.

NIR-II FGS was performed on the 3 patients with the fluorescence of tumor, with a complete resection rate of 100% (3/3, 95% CI 38.25% to 100%) achieved. However, in 4 patients with grade III gliomas who underwent WLS, the complete resection rate was only 25% (1/4, 95% CI 3.41% to 71.09%). No recurrence was observed in patients from both of the groups.

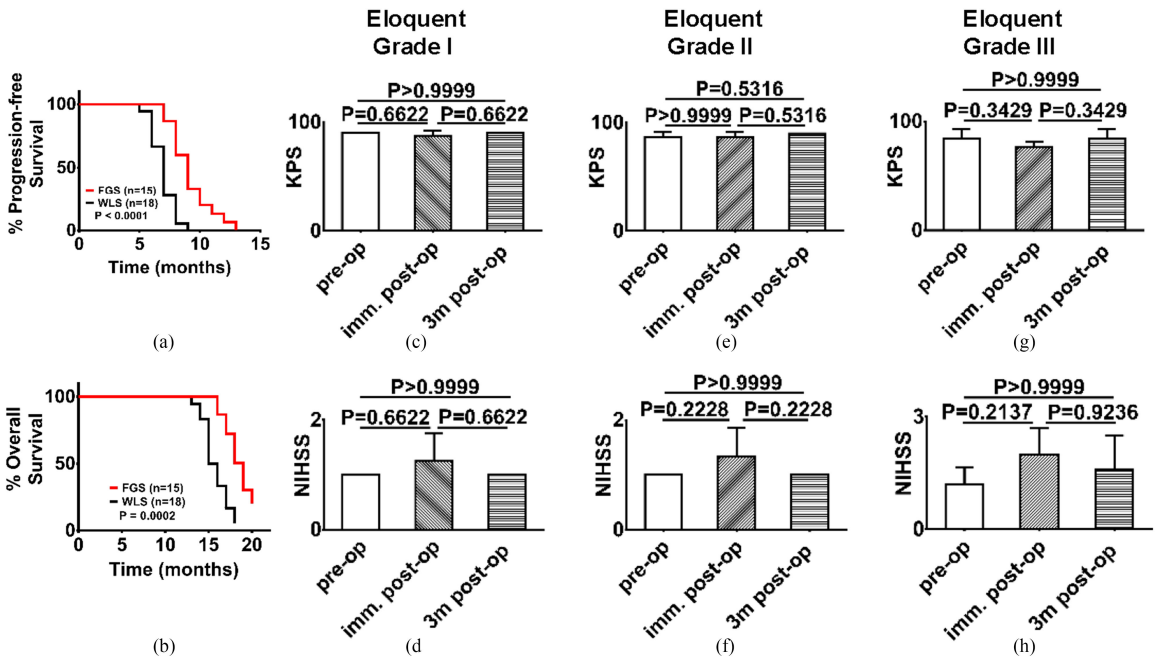

Fig. 5. PFS, OS, and neurological function of patients. (a)–(b), PFS (a) and OS (b) of the FGS group was significantly prolonged compared with the WLS group (PFS, $P < 0.0001$; OS, $P = 0.0002$). (c)–(h), KPS (row 1) and NIHSS (row 2) of patients in the FGS group with eloquent grade I lesions (n = 4, column 1), patients with eloquent grade II lesions (n = 7, column 2) and patients with eloquent grade III lesions (n = 4, column 3).

G. Reservation of Neurological Function During Surgery Using NIR-II FGS

NIR-II FGS demonstrated the potential to protect neurological function. After the gross tumor was removed, the residual NIR-II fluorescence provided the surgeons with precise guidance of the residual tumor, which helped to discriminate the residual tumor from surrounding normal brain tissue, and avoided unnecessary resection. And the samples of tissues with residual fluorescent signal were diagnosed to be tumor tissues. The median Karnofsky Performance Scale (KPS) and National Institute of Health Stroke Scale (NIHSS) 3 months after surgery were 90 and 1, respectively, in both groups. No significant difference was observed in patients of the FGS group with different grades of eloquent area infiltration for both KPS and NIHSS (Fig. 5(c)–(h) and Table IV). The same result was observed in patients of the WLS group (Table IV).

Impressively, an important case with WHO grade III glioma showed that the intraoperative NIR-II fluorescence images helped to avoid paralysis. The pre-operative T1-enhanced MRI exhibited enhancement in the left parietal-frontal lobe (Fig. S2 (a), left, labeled as pre-op). The patient was diagnosed to have a high risk of paralysis of his right limbs after surgery. The post-operative T1-enhanced MRI displayed no enhancement, which showed total resection of the tumor (Fig. S2 (a), right, labeled as post-op). After opening the dura, the position of the tumor was visualized by the tumor fluorescence penetrating through the intact cortex (Fig. S2 (b), row 1, labeled as pre-op). Then the gross tumor was removed very carefully. After that, the color and NIR-II/I fluorescence images of the operation field were acquired, displaying the tissue with residual NIR-II fluorescent signal (Fig. S2 (b), row 2, labeled as residual). The tissue with residual NIR-II fluorescent signal was further removed until no NIR-II fluorescence was left (Fig. S2 (b), row 3, labeled as post-op). The *in vivo* TNRs of NIR-II were higher than those of NIR-I for both pre-op and residual (Fig. S2 (c)), which indicated that NIR-II fluorescence images displayed the residual fluorescent signal more obviously. The color and NIR-II/I fluorescent images of the sample from the gross tumor (Fig. S2 (d), row 1) and the tissue with residual fluorescence (Fig. S2 (d), row 2) also showed obvious *ex vivo* NIR-II and NIR-I

TABLE IV
COMPARISON OF NEUROLOGICAL FUNCTION FOR FGS AND WLS GROUP

KPS		pre-op	imm. post-op	3 m. post-op	*P* value
FGS	Grade I	90.00±0.00	87.50±4.33	90.00±0.00	0.3678
	Grade II	86.67±4.71	86.67±4.71	90.00±0.00	0.2969
	Grade III	84.00±8.00	76.00±4.90	84.00±8.00	0.1896
WLS	Grade I	92.50±4.33	87.50±4.33	92.50±4.33	0.2937
	Grade II	88.57±3.50	87.14±4.51	88.57±3.50	0.7451
	Grade III	82.86±7.00	74.28±4.95	77.14±4.52	0.0694
NIHSS		pre-op	imm. post-op	3 m. post-op	*P* value
FGS	Grade I	1.00±0.00	1.25±0.43	1.00±0.00	0.3678
	Grade II	1.00±0.00	1.33±0.47	1.00±0.00	0.1194
	Grade III	1.20±0.40	2.00±0.63	1.60±0.80	0.1945
WLS	Grade I	0.75±0.83	0.75±0.83	0.75±0.83	1.0000
	Grade II	1.00±0.00	1.28+0.45	1.00±0.00	0.1218
	Grade III	0.85±0.35	2.00±0.53	2.00±0.53	0.0021

FGS, fluorescence image-guided surgery; WLS, white light image-guided surgery; KPS, Karnofsky performance score; NIHSS, National Institutes of Health Stroke Scale; pre-op, pre-operative measurement; imm. post-op, immediate post-operative measurement; 3 m. post-op, 3 months post-operative measurement.

fluorescent signal, with the histopathological diagnosis proved the sample to be WHO grade III and grade II, respectively. The motor function of the patient was successfully reserved by the guidance of NIR-II imaging (Supplementary movie).

IV. Discussion

In this study, the imaging performance and treatment efficacy of NIR-II based FGS have been evaluated in human glioma resection surgery using our in-house developed multispectral imaging system and FDA approved ICG probe. The FGS has been demonstrated to be a promising intraoperative real-time imaging technique for localizing GBM and residual tumors with high safety, high sensitivity, and real-time feedback. The properties of low photon scattering and absorption of tissue render the NIR-II fluorescence with a strong capability to detect tumors of larger depth. More importantly, our study clearly demonstrates that NIR-II based FGS achieves significant clinical benefits. The detection rate of the NIR-II FGS is 100% in patients with GBM. Moreover, compared with the WLS technique, the use of FGS lead to a dramatically improved complete resection rate (100% [95% CI 73.41-100] *vs.* 50% [95% CI 29.03-70.97], $P = 0.0036$) and significantly prolonged PFS and OS (PFS, $P < 0.0001$ and OS, $P = 0.0002$). The postoperative KPS and NIHSS measurements of the two groups also show no damage to the neurological function, indicating that the FGS is a safe technique and provides significant benefits to GBM patients.

It has been found that the complete resection rate of the FGS group is significantly higher than that of the WLS group in our study. Moreover, ICG based NIR-II FGS also performs better than 5-ALA, FS based FGS, and ICG based conventional NIR-I FGS in complete resection rate as reported previously [17], [20], [24]. In our study, the patients without residual fluorescence all achieve complete resection, demonstrating a complete resection rate of 100% (13/13). For the rest 2 patients without complete resection, residual tissue with fluorescence has been observed intraoperatively and reserved in order to conserve the neurological function of patients. Signal enhancement has also been observed in the postoperative enhanced MRI for these two patients. Whereas, complete resection rate of 50% (9/18) has been achieved in the WLS group, which is only half of the FGS group. Furthermore, the ICG based NIR-II FGS also out-performs 5-ALA and FS according to previous reports, as complete resection rate of ICG based NIR-I FGS reported in a study involving 15 patients with GBM is only 53.33% (8/15) [24] and that of 5-ALA and FS based FGS is 64.75% (90/139) and 82.60% (38/46) respectively [17], [20]. In a recently reported study of 5-ALA based FGS, only 3 out of 16 patients enrolled achieved complete resection, resulting in a complete resection rate to be 18.7% [28]. All of them are much lower than the complete resection rate (100%) of ICG based NIR-II FGS revealed in this study. The NIR-II fluorescence imaging technique can provide the surgeons with an accurate prompt of residual tumor, resulting in improved EOR and more complete resection. Previous studies suggest that improved EOR is beneficial to survival [7]. Therefore, ICG NIR-II imaging with a high complete resection rate of GBM greatly benefit the survival of patients.

Impressively, the PFS and OS has been prolonged in the NIR-II FGS group compared with the WLS group, and also with that of 5-ALA and FS based FGS reported previously. In our study, the median PFS of the FGS and WLS group was 9.0 months and 7.0 months, respectively. Median OS of 19.0 months and 15.5 months were achieved by FGS and WLS groups. However, median PFS and OS of 5.1 and 15.2 months in 139 patients for 5-ALA based fluorescence image-guided surgery were reported [17]. The median PFS and OS of FS based fluorescence image-guided surgery were 7 and 12 months [20]. In the most recent report of 5-ALA based fluorescence image-guided surgery, the mean PFS and OS were reported to be 5 ± 3 and 6.3 ± 4.6 months [28]. The 6m-PFS of the NIR-II FGS group is reported much higher than that of the WLS group (100% [95% CI 76.14-100.00] *vs.* 66.67% [95% CI 43.57-83.90], $P = 0.0134$), with a difference between the groups of 33.33%. Compared with 5-ALA based FGS reported, the NIR-II FGS has an even much higher 6m-PFS (100% *vs.* 41.0% and 46.2%) [17], [28]. For FS based FGS, 6m-PFS has been reported to be only 56.6% [20], which is 43.4% lower than that of the NIR-II FGS. Therefore, the PFS of the ICG based NIR-II FGS is prolonged compared with the previously reported 5-ALA and FS based FGS. It should be pointed out that the uncompleted total Stupp protocol in previous studies due to the medical condition when the trials were performed is unignorable when analyzing the survival of patients. Besides, although significant improvement of survival has already been achieved in our trial reported in the manuscript, the increase of 2 months and 3.5 months for PFS and OS is still less effective. The reasons are older age and IDH wild type of the patients enrolled in the trial. On the one hand, the mean ages of patients were 51.73 ± 11.24 for the FGS group and 53.83 ± 14.73 for the WLS group. As reported most recently, such an older age is a risk factor for shorter OS [29]. On the other hand, 14 of the 15 patients in the FGS group and 16 in the 18 patients in the WLS group were IDH wild type, which was reported to have shorter OS compared with IDH mutant type (IDH wild type, 1.2 years vs. IDH mutant type, 3.6 years) [30].

It is also worthy to note that in the previous study of ICG based NIR-I FGS, a dose of 5mg/kg has been administrated to the patients, with no significant acute toxicity observed [24]. In this study, the dose of ICG used in the FGS group is dramatically reduced to 1mg/kg, which is only twice the dose commonly used in clinical. Moreover, this dose is also much lower compared with the previous study reported (5mg/kg) [24]. No specific adverse event has been observed. The liver enzymes have been monitored before and after surgery, with no abnormal value observed. The best imaging time window has been explored in limited patients with such a low dose and finally set to be 48 h after injection. Although the NIR-II performs better and benefits more to the patients, our study also reveals a limitation of ICG based NIR-II fluorescence imaging for GBM. As ICG cannot specifically target GBM, the NIR-II fluorescence imaging based on ICG is also not specific for glioblastoma. The adjacent non-tumor tissue is possible to uptake ICG by diffusion

or hyperplastic blood vessels, which causes the existence of false positives. It is reported that a fluorescent probe based on bombesin has shown high specificity for human glioma detection [31]. Thus, a targeted NIR-II probe will be prepared and explored in our future studies, which may further improve the clinical value of the NIR-II imaging technique for glioma detection and image-guided surgery.

V. Conclusion

In summary, our study demonstrates the feasibility of using NIR-II FGS in GBM resection. The ICG based NIR-II fluorescence can be observed in all the GBM patients involved in FGS. More importantly, with the guidance of NIR-II fluorescence images, the complete resection rate can be dramatically improved without damaging neurological functions. The NIR-II FGS technique can achieve a high 6m-PFS and greatly prolong the PFS and OS of the GBM patients. Moreover, *ex vivo* NIR-II fluorescence imaging outperforms NIR-I imaging and surgeons' diagnosis under white light in sample discrimination. It possesses high sensitivity and NPV and provides a convincing diagnosis of whether the tissue is a tumor. Overall, NIR-II FGS is a highly promising technique worthy of exploring more clinical applications.

References

[1] P. Diamandis and K. Aldape, "World health organization 2016 classification of central nervous system tumors," *Neurol. Clin.*, vol. 36, no. 3, pp. 439–447, Aug. 2018.

[2] Q. T. Ostrom *et al.*, "CBTRUS statistical report: Primary brain and other central nervous system tumors diagnosed in the United States in 2012–2016," *Neuro-Oncology*, vol. 21, no. Suppl 5, pp. V1–V100, Oct. 2019.

[3] B. M. Alexander and T. F. Cloughesy, "Adult glioblastoma," *J. Clin. Oncol.*, vol. 35, no. 21, pp. 2402–2409, Jul. 2017.

[4] A. S. Jakola *et al.*, "Comparison of a strategy favoring early surgical resection vs a strategy favoring watchful waiting in low-grade gliomas," *JAMA*, vol. 308, no. 18, pp. 1881–1888, Nov. 2012.

[5] K. L. Chaichana *et al.*, "Recurrence and malignant degeneration after resection of adult hemispheric low-grade gliomas," *J. Neurosurgery*, vol. 112, no. 1, pp. 10–17, Jan. 2010.

[6] N. Sanai and M. Berger, "Surgical oncology for gliomas: The state of the art," *Nature Rev. Clin. Oncol.*, vol. 15, no. 2, pp. 112–125, Feb. 2018.

[7] R. S. D'Amico *et al.*, "Extent of resection in glioma–a review of the cutting edge," *World Neurosurgery*, vol. 103, pp. 538–549, Jul. 2017.

[8] E. Belykh *et al.*, "Intraoperative fluorescence imaging for personalized brain tumor resection: Current state and future directions," *Front. Surg.*, vol. 3, p. 55, Oct. 2016.

[9] D. W. Roberts *et al.*, "Intraoperative brain shift and deformation: A quantitative analysis of cortical displacement in 28 cases," *Neurosurgery*, vol. 43, no. 4, pp. 749–758, Oct. 1998.

[10] S. Hu *et al.*, "Real-time imaging of brain tumor for image-guided surgery," *Adv. Healthcare Mater.*, vol. 7, no. 16, Aug. 2018, Art. no. 1800066.

[11] C. Qin *et al.*, "Recent advances in Cerenkov luminescence and tomography imaging," *IEEE J. Sel. Topics Quantum Electron.*, vol. 18, no. 3, pp. 1084–1093, Jul. 2011.

[12] Z. Zhang *et al.*, "Endoscopic Cerenkov luminescence imaging and image-guided tumor resection on hepatocellular carcinoma-bearing mouse models," *Nanomedicine*, vol. 17, pp. 62–70, Apr. 2019.

[13] H. Guo *et al.*, "A hybrid clustering algorithm for multiple-source resolving in bioluminescence tomography," *J. Biophotonics*, vol. 11, no. 4, Jul. 2017, Art. no. e201700056.

[14] S. Zheng *et al.*, "Radiopharmaceuticals and fluorescein sodium mediated triple-modality molecular imaging allows precise image-guided tumor surgery," *Adv. Sci.*, vol. 6, no. 13, Jul. 2019, Art. no. 1900159.

[15] M. Liu *et al.*, "Cerenkov luminescence imaging on evaluation of early response to chemotherapy of drug-resistant gastric cancer," *Nanomedicine*, vol. 14, no. 1, pp. 205–213, Jan. 2018.

[16] W. Si *et al.*, "Assessing performance of augmented reality-based neurosurgical training," *Visual Comput. Ind., Biomed., Art*, vol. 2, no. 1, pp. 1–10, Jul. 2019.

[17] W. Stummer *et al.*, "Fluorescence-guided surgery with 5-aminolevulinic acid for resection of malignant glioma: A randomised controlled multicentre phase III trial," *Lancet Oncol.*, vol. 7, no. 5, pp. 392–401, May 2006.

[18] S. K. Kim *et al.*, "Impact of fluorescence-guided surgery on the improvement of clinical outcomes in glioblastoma patients," *Neuro-Oncology Pract.*, vol. 1, no. 3, pp. 81–85, Sep. 2014.

[19] R. D. Valle, C. G. Hadjipanayis, and W. Stummer, "Established and emerging uses of 5-ALA in the brain: An overview," *J. Neuro-Oncology*, vol. 141, no. 3, pp. 487–494, Feb. 2019.

[20] F. Acerbi *et al.*, "Fluorescein-guided surgery for resection of high-grade gliomas: A multicentric prospective phase II study (FLUOGLIO)," *Clin. Cancer Res.*, vol. 24, no. 1, pp. 52–61, Jan. 2018.

[21] B. Kiesel *et al.*, "Systematic histopathological analysis of different 5-aminolevulinic acid–induced fluorescence levels in newly diagnosed glioblastomas," *J. Neurosurgery*, vol. 129, no. 2, pp. 341–353, Oct. 2017.

[22] R. J. Diaz *et al.*, "Study of the biodistribution of fluorescein in glioma-infiltrated mouse brain and histopathological correlation of intraoperative findings in high-grade gliomas resected under fluorescein fluorescence guidance," *J. Neurosurgery*, vol. 122, no. 6, pp. 1360–1369, Jun. 2015.

[23] A. Ergin *et al.*, "The feasibility of real-time in vivo optical detection of blood–brain barrier disruption with indocyanine green," *J. Neuro-Oncology*, vol. 106, no. 3, pp. 551–560, Feb. 2012.

[24] J. Y. K. Lee *et al.*, "Intraoperative near-infrared optical imaging can localize gadolinium-enhancing gliomas during surgery," *Neurosurgery*, vol. 79, no. 6, pp. 856–871, Dec. 2016.

[25] J. A. Carr *et al.*, "Shortwave infrared fluorescence imaging with the clinically approved near-infrared dye indocyanine green," *Proc. Nat. Acad. Sci. USA*, Apr. 2018, vol. 115, no. 17, pp. 4465–4470.

[26] Z. Hu *et al.*, "First-in-human liver-tumour surgery guided by multispectral fluorescence imaging in the visible and near-infrared-I/II windows," *Nature Biomed. Eng.*, vol. 4, no. 3, pp. 259–271, Mar. 2020.

[27] C. W. Teng *et al.*, "Applications of indocyanine green in brain tumor surgery: Review of clinical evidence and emerging technologies," *Neurosurg Focus*, vol. 50, no. 1, Jan. 2021, Art. no. E4.

[28] G. A. Maragkos *et al.*, "Fluorescence-guided high-grade glioma surgery more than four hours after 5-aminolevulinic acid administration," *Front. Neurol.*, vol. 12, Mar. 2021, Art. no. 644804.

[29] N. Kudulaiti *et al.*, "A nomogram for individualized prediction of overall survival in patients with newly diagnosed glioblastoma: A real-world retrospective cohort study," *BMC Surg.*, vol. 21, no. 1, pp. 238, May 2021.

[30] A. M. Molinaro *et al.*, "Association of maximal extent of resection of contrast-enhanced and non-contrast-enhanced tumor with survival within molecular subgroups of patients with newly diagnosed glioblastoma," *JAMA Oncol.*, vol. 6, no. 4, pp. 495–503, Apr. 2020.

[31] D. Li *et al.*, "First-in-human study of PET and optical dual-modality image-guided surgery in glioblastoma using 68Ga-IRDye800CW-BBN," *Theranostics*, vol. 8, no. 9, pp. 2508–2520, 2018.